A measurement-based fading model for wireless personal area networks

Kåredal, Johan; Johansson, Anders J; Tufvesson, Fredrik; Molisch, Andreas

Link to publication

A Measurement-Based Fading Model for Wireless Personal Area Networks

Johan Karedal, *Student Member, IEEE*, Anders J. Johansson, *Member, IEEE*,
Fredrik Tufvesson, *Senior Member, IEEE*, and Andreas F. Molisch, *Fellow, IEEE*

Abstract—Personal area networks (PANs) are wireless communications systems with high data rates but small coverage area. PAN propagation channels differ from the well-explored propagation channels of wide-area networks due to several reasons: (i) the distances are typically very small, (ii) the antenna arrangements can be quite different, and (iii) the influence from human presence in the environment is different.

The current paper presents results of a channel measurement campaign, where measurements are conducted over distances of 1-10 m using several multi-antenna devices, combined to create different PAN scenarios. For each measured Tx-Rx separation, channel realizations are obtained by small spatial movements of the antenna devices, and by rotating the persons holding the devices.

From the results, we draw two main conclusions: (i) The small-scale amplitude statistics, analyzed as the variations over a small sampling area and frequency subchannels, cannot be described in a satisfactory way using only the Rayleigh or Ricean distribution, rather a mixed distribution, the generalized gamma distribution, is more suitable; (ii) it is advantageous to distinguish between two types of large-scale fading: body shadowing (due to the orientation of the person holding the device) and shadowing due to surrounding objects (lateral movement). We also define and parameterize a complete statistical model for all fading.

Index Terms—Personal area networks, channel measurements, statistical channel model, body shadowing.

I. INTRODUCTION

PERSONAL area networks (PANs) are often defined as a network where transmitter and receiver are separated no more than 10 m, usually located within the same room. In the last years, there has been a steadily increasing interest in such networks, and various technologies have been explored for improving their performance [3], [4]. In order to achieve the high data rates that are required for many PAN applications, multiple-antenna systems [5], [6], [7] seem especially suitable and have been explored, e.g., in the European MAGNET project [8].

In order to assess the potential and the performance of PAN systems, it is necessary to measure and model the wireless propagation channels between transmitters and receivers. PAN channels differ remarkably from traditional wireless local area network (WLAN) channels that have been well explored. First, the distance between transmitter and receiver is smaller for PANs than in typical WLANs. Secondly, most multi-antenna WLAN propagation channel measurement campaigns make use of uniform arrays, in which the physical environment experienced by an array element can also be assumed to be experience by its array neighbor. However, the antenna arrangements on PAN devices can be quite different, with antenna elements being squeezed in wherever they may fit, and thus different antenna elements can no longer be expected to "see" the same environment. Thirdly, and most importantly, PAN communications usually involve at least one handheld or bodyworn device, and the user holding the device has a distinctive impact on the propagation channel. The user can be viewed as an integral part of antenna, i.e., the total antenna pattern is determined by a combination of the exact positions of the antenna, the user and his/her extremities. Therefore, it is preferable to analyze the combined effect of channel, antennas, and human operators of the mobile station - again in contrast to WLAN channels, where models of propagation channels in the absence of users are the norm (see, e.g., [9]).[1]

While there are numerous publications on BAN propagation (see, e.g., [11], [12] and [13]), the propagation effects in PAN settings are quite different, and despite their great practical importance, measurements and models of PAN channels can, to the authors' best knowledge, hardly be found in the literature. The current paper intends to alleviate that gap. It reports the results of a wideband measurement campaign for a number of PAN scenarios, where we find that PAN channels show a fundamentally different *structure* of the small-scale and the large-scale fading.

Large-scale fading or shadowing, i.e., variations of the received power due to obstruction of propagation paths by various objects, has commonly been modeled as lognormally-distributed variations of the (distance-dependent, narrowband) pathloss. However, this model was originally devised for cellular systems, and is insufficient for many PANs; due to the body shadowing, variations occur not only by lateral movement, but also by rotation of the user (which are more common in PANs), and/or movement of the antennas with respect to the body. It is thus preferable to distinguish between the shadowing caused by surrounding objects and the shadowing

[1]An exception is, e.g., the recent paper [10] that analyzes the impact of humans on the transfer function in wireless LANs.

caused by the body as different types of movements of the users lead to different types of shadowing, with different fading statistics and coherence times.

Small-scale fading is typically modeled as being Ricean distributed for line-of-sight (LOS) situations, and Rayleigh distributed for non-line-of-sight (NLOS) situations. However, as we will see in this paper, the proximity of the human body and the irregular antenna arrangements, makes this description insufficient, and furthermore, the antenna arrangements also cause the small-scale fading to have different statistics at different antenna elements.

Thus, the key contributions of this paper are:

- We present results from an extensive measurement campaign performed in a modern office building for PAN propagation channels. The measurement campaign covers two frequency bands (center frequencies of 2.6 and 5.2 GHz).
- We compare the results for several different PAN scenarios, using several different types of multi-antenna devices (access points, handheld devices, laptops and a bodyworn device).
- We show the impact of typical antenna arrangements, as well as the influence of the human operator of the antenna device. Especially, we find that the generalized gamma distribution should be used to describe the small-scale fading, since neither Rayleigh nor Ricean distributions give a satisfactory description of the fading statistics.
- We introduce and motivate a distinction between body-shadowing and environment shadowing, and experimentally verify this concept.
- We provide a complete statistical model for the two types of shadowing and the small-scale fading statistics.

Though all measurements in our campaign are done with multiple-antenna devices, an evaluation of MIMO correlation matrices and resulting capacity analysis is relegated to a separate paper.

The remainder of the paper is organized the following way: Section II describes the setup for the measurements, and the physical environment in which the measurements were made. Section III describes the model parameters as well as how they are extracted from the measurements. Also, a discussion about the different types of shadowing, and explanations why different types of movement lead to different values of shadowing is included. Section IV presents measurement results and extracted channel parameters of interest, whereas Section V describes our model based on the results from the previous section. Finally, a summary and conclusions in Section VI wraps up this paper.

II. MEASUREMENT SETUP

The measurements were done with the RUSK LUND channel sounder that performs MIMO measurements based on the "switched array" principle [14]. Two different frequency bands were investigated, 2.6 ± 0.1 GHz and 5.2 ± 0.1 GHz, each of which was measured at 321 equidistantly spaced frequency points. The RUSK sounder allows to adjust the length of the test signal, and for these measurements a value of 1.6 μs was used, corresponding to a resolvable "excess runlength" of
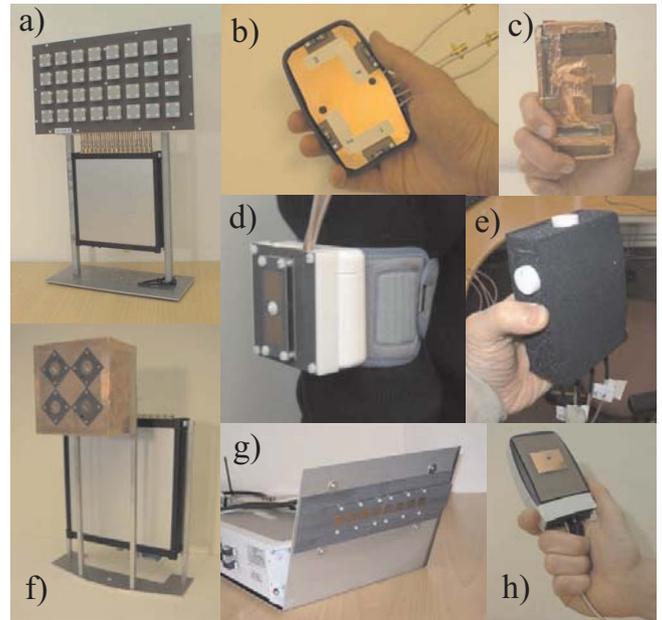

Fig. 1. The antennas used in the measurements: a) 2.6 GHz access point; b) 2.6 GHz 4-element handheld device (with the plastic lid removed in order to expose the antennas); c) 5.2 GHz 4-element handheld device; d) 5.2 GHz bodyworn device; e) 5.2 GHz 6-element handheld device; f) 5.2 GHz access point; g) laptop dummy, here with the 5.2 GHz array mounted; h) 2.6 GHz 2-element handheld device.

multipath components of 480 m, which was more than enough in our considered environment to avoid overlap of subsequent impulse responses. In order to gather a large number of channel samples, the receiver unit was slowly moved over a small area during each measurement (details of the movement will be described in Sec. II-C) allowing the channel sounder to record 10 different channel samples, or snapshots, with small spatial offsets. The output power of the channel sounder was 0.5 W, and we made sure that the received signal level always was within the allowable limits of the sounder.

Several antenna arrays were used for each frequency band. The different arrays where designed with an intention of resembling realistic multi-antenna consumer devices as much as possible. Hence, we used access point (AP) arrays, hand-held (HH) device arrays (similar to personal digital assistants, PDAs, or mobile phones), laptop computer (PC) arrays and a body worn (BW) device array (similar to a blood-pressure gauge) and by using different combinations of antenna devices as Tx and Rx, four different scenarios were created. The following sections describe the different antenna arrays, the measurement environment and the scenarios in greater detail.

A. Antenna Devices

In total, 11 different antenna devices were used throughout the measurement campaign (see Fig. 1). Hereinafter, the array size is, where applicable, given as (number of rows × number of columns × number of polarizations per antenna element).

1) Access Point – 2.6 GHz: The 2.6 GHz access point was a $(4 \times 8 \times 2)$ antenna array consisting of quadratic, dual-polarized, microstrip antennas. Only the middle two rows were used during the measurements, and the ports of the other two where terminated with 50 Ω-terminations. The array

was tripod-mounted at ceiling height in order to increase the resemblance with a real access point.

2) Laptop Computer – 2.6 GHz: This device consisted of a $(1 \times 4 \times 2)$ array of the same sort of elements as the 2.6 GHz AP, mounted on a laptop dummy (a laptop-shaped metal frame). The array was placed on the reverse side of the "screen", with the broadside direction aiming away from the "keyboard". Since the "screen" was tilted slightly backwards (in order represent a typical laptop pose), so was the antenna array.

3) Handheld Device – 2.6 GHz: Two different handheld devices were used, one with 2 elements and one with 4 elements. The latter device, used in the AP/HH/PC to HH scenarios, consisted of a plastic box containing a ground plane and 4 PIFAs, one on each edge of the ground plane. The element on the rightmost edge (see Fig. 1b) was constantly covered by the hand during the measurements and was therefore disregarded in the analysis. The 2-element array, used only in the HH to HH scenario, consisted of an identical plastic box, equipped with 2 rectangular patch antenna elements with orthogonal polarization, mounted on opposite sides on the outside of the box (see Fig. 1h).

4) Access Point – 5.2 GHz: A $(2 \times 2 \times 2)$ array of dual-polarized, circular microstrip antennas was used as the 5.2 GHz access point, tripod-mounted in the same way as in the 2.6 GHz case.

5) Laptop Computer – 5.2 GHz: The metal frame of the corresponding 2.6 GHz scenario was also used at 5.2 GHz, though equipped with a $(1 \times 8 \times 2)$ array of dual-excited microstrip element.

6) Handheld Device – 5.2 GHz: Four antenna devices, of two different types, were used. The first type of HH was a 4-element slot antenna array (denoted HH_4), consisting of a metal box with built-in slot antenna elements; two in the front of the box, perpendicular to each other, one in the top side, and one in the right side of the box. The front left element of one HH_4 was found to give abnormal results, and was therefore disregarded in the analysis. This device is thus denoted HH_3. The second type of HH was a 6-element circular patch antenna array (denoted HH_6). Three dual-polarized antennas were mounted outside a foam-clad metal box; one on the left side, one on the top side, and one on the right side.

7) Bodyworn Device – 5.2 GHz: As a bodyworn device, we used a $(2 \times 1 \times 2)$ array of the same type of microstrip elements used for the 5.2 GHz PC. The array was mounted on top a plastic box (originally a blood-pressure gauge), attached to a strip of Velcro tape enabling wearing of the device.

B. The Office Environment

The measurements were performed in an office environment in the E-building at Lund University, Lund, Sweden. Office floor sizes are between 10 m^2 and 30 m^2, where the outer walls of the building consist of brick and reinforced concrete, whereas gypsum wallboards separate different offices. Throughout the offices, different Tx and Rx positions were selected to constitute realistic usage situations with a Tx-Rx separation less than 10 m. All scenarios could not share the exact same set of positions, since what is regarded as a realistic
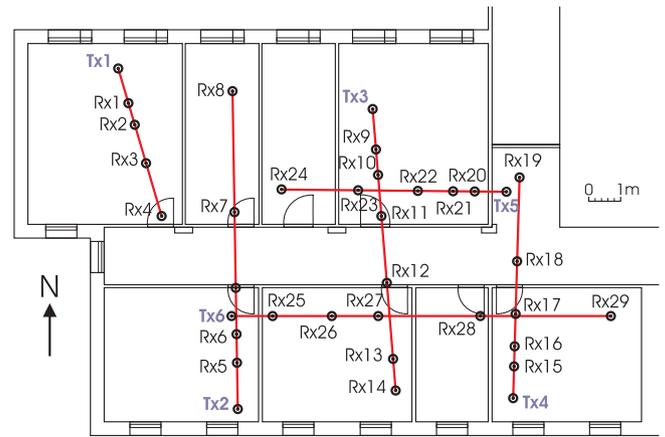

Fig. 2. Site map of the measurement positions for the HH to HH scenarios. Measurements were only recorded between positions along the lines.

position for a certain type of antenna device, may not be very realistic for another. The same set of positions was used for the AP to HH and AP to BW measurements, whereas the PC to HH scenario only used a subset of these. The HH to HH scenarios used their own set of positions, as shown in Fig. 2.

The shadowing impact of the human operator discussed earlier also leads to an ambiguity in the definition of "line-of-sight" (LOS), as it is not obvious if a channel where the shortest propagation path between Tx and Rx is obstructed by one or several human operators should be counted as LOS or not. We choose to separate our measurements into LOS and NLOS according to a definition where a measurement is considered LOS when the *operators* are within line-of-sight of each other.

C. Measurement Scenarios

In this section we describe the different measurement scenarios; the common features of the various setups are summarized in Table I, where N_{meas} is the total number of measurements per scenario, N_{Tx} the number of Tx positions and N_{Rx} the number of Rx positions (given as LOS/NLOS). Furthermore, "Tx or." and "Rx or." are the measured Tx/Rx orientations, respectively.

1) Access Point to Handheld Device (AP2HH): In this scenario, the AP was used as Tx. Five different Tx/AP positions were selected amongst the offices along with 20 Rx/HH positions. Three AP positions were used for NLOS measurements, whereas two were used to create LOS situations. For each NLOS Tx position, measurements were made at every (NLOS) HH position within a 10 m range, whereas for the LOS AP positions, measurements were made at each HH position within LOS. During the measurements, the HH was held by a person seated in front of a desk (at 5.2 GHz, the HH_3 and one HH_6 was simultaneously held, one in each hand), and in order to capture the effects of orientation with respect to the AP as well as the shadowing of the operator's body, four different measurements were made at every HH position. These measurements were made with different orientations of the person holding the HH; orientations of $0°$ (the person facing the desk), $90°$, $180°$ and $270°$ were measured. In order to obtain ten channel snapshots, the human operator moved

TABLE I
MEASUREMENT SCENARIOS.

Scenario	N_{meas}	Tx unit	N_{Tx}	N_{Rx}	Tx or.	Rx or.		
AP2HH	44/192	AP	2/3	11/18	–	$0°, 90°, 180°, 270°$	rel. to	desk
PC2HH	96/–	PC	5/–	19/–	–	$0°, 90°, 180°, 270°$	rel. to	desk
HH2HH	180/90	HH	4/2	20/10	$60°, 180°, 300°$	$60°, 180°, 300°$	rel. to	Rx/Tx
AP2BW	44/124	AP	2/2	11/18	–	$0°, 90°, 180°, 270°$	rel. to	desk

the HH(s) in front of his body over an area of approximately 30×30 cm^2.

2) Laptop Computer to Handheld Device (PC2HH): This scenario used the PC as Tx and was limited to LOS measurements only. Five Rx positions of the AP to HH scenario, one in each office, were used as Tx/PC positions, and measurements were made at all HH positions within LOS. The stance of the person holding the antenna(s) (the HH$_3$ and one HH$_6$ at 5.2 GHz) the principle of measuring four different orientations of the antenna carrier, and the obtaining of ten channel snapshots were the same as for the AP to HH scenario.

3) Handheld Device to Handheld Device (HH2HH): For the HH to HH scenario, both Tx and Rx were held by standing persons (at 5.2 GHz, either person was equipped with a HH$_{3/4}$ *and* a HH$_6$). LOS situations were created using 4 Tx and 20 Rx positions, whereas NLOS measurements were made with 2 Tx and 10 Rx positions (see Fig. 2). Similar to previous scenarios, measurements with different antenna orientations were made in order to capture the effects of body shadowing. In this scenario, however, both Tx *and* Rx (or rather the antenna-carrying persons) were varied over an ensemble of different orientations; $60°$, $180°$ and $300°$ (with $0°$ denoting the bearing to the other antenna carrier). Hence, nine measurement were made for every Tx-Rx position. Ten snapshots were obtained by moving the Rx device(s) in the same way as in the AP to HH scenario.

4) Access Point to Bodyworn Device (AP2BW): In the AP to BW scenario, the AP was used as Tx. The measurement points as well as the orientations of the antenna device carrier were the same as in the AP to HH scenario (though one Tx position less was used for NLOS). The BW was carried around the right biceps of the carrier, facing away from the body. To obtain ten channel snapshots, the carrier moved his torso slowly over an area of approximately 30×30 cm^2 during the measurements.

III. MODEL PARAMETERS AND DATA EVALUATION

The standard model for fading, i.e., fluctuations in the received power of a wireless channel, is the combined effect of two processes: the small-scale fading and the large-scale fading, also known as shadowing [15]. The former is due to the constructive and destructive interference of the multipath components (MPCs) impinging of the receiver, and is thus related to the relative *phases* of the multipath components. The latter is due to changes in the average *power* of the multipath components; it is typically assumed to be due to large-scale variations in the physical environment of the receiver. Since the channel sounder performs measurements in the frequency domain, we have for each measurement location (with a Tx-Rx separation d; consisting of O orientations each consisting of $S = 10$ snapshots), a channel transfer function for snapshot

s of orientation o of the transmission between Rx element m and Tx element n defined as $H = H(f, d, o, s, m, n)$. Based on the transfer functions, we extract information about the fading as described in the subsequent sections.

A. Shadowing

Traditionally, variations of the shadowing are assumed to occur when the mobile station moves (laterally) over large distances, and are described as a random process with a lognormal amplitude probability density function. In PANs a strong impact of the human presence in the near field of its antennas can be expected and hence one or several human bodies are likely to lead to shadowing in a wireless PAN channel. Human presence in a wireless channel, even with handheld devices, is not a new problem and has been studied for cellular networks for quite some time. However, the common method of including the human impact is as a time-invariant "bulk attenuation factor" (see e.g., [16]); variations of the shadowing due to rotation by the user have to the best of our knowledge not been modeled statistically. Furthermore, PANs also show an additional mechanism for shadowing variations as the relative position between the body and a handheld device can change frequently.

We also note that the used device and antenna types affect the amount of shadowing inflicted by the human body, as the antenna patterns determine how much power will be received or transmitted through the body of the operator. It is also of importance where the antennas are mounted and how they are directed with respect to the body, and hence, the human body will, depending on the exact locations of Tx, Rx and human operator, add a different amount of shadowing on the received power. Thus, the assumption of the shadowing experienced by a receiver being constant for each Tx-Rx position is no longer valid: if a person rotates, the amount of shadowing will change markedly. The total shadowing induced by the channel will thus be the sum of two parts, and hence it is reasonable to separate two types of shadowing: 1) the power variations due to the physical surroundings around Tx and Rx, and 2) the power variations due to the changes of body shadowing induced by the operator of the device.

To investigate the influence of rotations and body shadowing, we determine the path gain for two cases: the *total* path gain $G_{\mathrm{tot}}(d)$ is defined as the average of $|H|^2$ over antennas, frequency, snapshots and orientation, while the *local* path gain $G_i(d, o)$ is defined as the average of $|H|^2$ over antennas, frequency and snapshots. By fitting a deterministic distance decay $G_{\mathrm{det}}(d)$ to describe the distance dependence of $G_{\mathrm{tot}}(d)$, the shadowing loss due to the environment, L_e, is defined as the local variation of $G_{\mathrm{tot}}(d)$ around $G_{\mathrm{det}}(d)$, and the shadowing loss due to the body/orientation, L_b, is defined as the local variations of $G_i(d, o)$ around $G_{\mathrm{tot}}(d)$.

B. Small-Scale Fading

The small-scale amplitude variations are analyzed from frequency domain data, i.e., from the channel transfer functions. On most antenna arrays that we use, different antenna elements have different directions or polarizations, and for that reason, separate small-scale analysis is done for each Tx-Rx antenna element pair (or *spatial channel*).

First, we want to characterize the relative path gain of each spatial channel, G_r, i.e., the mean power of each spatial channel (over snapshots and frequency) relative the mean power over all spatial channels within a measurement. Then, to evaluate the small-scale amplitude variations around G_r, we use an ensemble of frequency sub-channels *and* snapshots (i.e., 3210 channel samples) as the basis for analysis.[2] We normalize the amplitude data $r = |H|$ to unit power, i.e., $E(r^2) = 1$, fit the data to three possible distributions and select the best fit. The three candidate distributions we consider are the Rayleigh distribution, the Rice distribution and a mixed distribution to account for situations that are neither Rayleigh nor Ricean. While a number of different distributions are possible for the latter case, we choose here the generalized gamma (GG) distribution [18], whose pdf is

$$ p_R(r) = \frac{c r^{c\alpha - 1}}{\beta^{c\alpha} \Gamma(\alpha)} \exp\left[-\left(\frac{r}{\beta}\right)^c \right], \qquad (1) $$

where $\Gamma(\sim)$ is the Gamma function, because of its simple functional form. With a proper choice of its three parameters α, β and c, the GG distribution can represent a wide variety of distributions including the Rayleigh and the Rice case.[3] Fitting of the different distribution parameters is done by means of maximum-likelihood (ML) estimation. Since no closed-form expression exists for the Ricean K-factor, ML estimates are obtained by stepping through a range of values from 0.1 to 20 and selecting the one that maximizes the log-likelihood function. For the GG distribution, the ML estimates of α, β and c can be shown to fulfill [19]

$$ \hat{\beta} = \left(\frac{1}{N\hat{\alpha}} \sum_{n=1}^{N} x_n^{\hat{c}} \right)^{1/\hat{c}}, \qquad (2) $$

$$ \frac{1}{\hat{\alpha}} = \hat{c} \left(\frac{\sum_{n=1}^{N} x_n^{\hat{c}} \ln x_n}{\sum_{n=1}^{N} x_n^{\hat{c}}} - \frac{1}{N} \sum_{n=1}^{N} \ln x_n \right). \qquad (3) $$

Numeric ML estimates can thus be derived by stepping through a range of c-values (from 0.1 to 10), determining the corresponding α and β from Eqs. (2) and (3), and selecting the set of $\{\alpha, \beta, c\}$ that maximizes the log-likelihood function.

After deriving the ML estimates of the parameters for each candidate distribution, we use Akaike's Information Criterion (AIC) [20] to derive its corresponding Akaike weight. As the latter is interpreted as the probability that the candidate distribution gives the best fit, we thus regard the pdf with the largest weight as the one giving the best fit to our data.

[2]With the delay spreads we measure in these scenarios (10–12 ns), the corresponding (0.5–)coherence bandwidth ensures that we have enough independent frequency samples for the analysis (the measured bandwidth of 200 MHz implies 11–13 independent samples per snapshot, i.e., a total of 110–130 per ensemble) [17].

[3]Though the Rice pdf cannot be *exactly* represented by a generalized gamma, it indeed constitutes a very good approximation [18].

C. Delay Dispersion

In order to analyze the delay dispersion of the channel, we convert the channel transfer functions to impulse responses by means of an inverse Fourier transform (using a Hanning window) from which we derive the averaged power delay profiles (APDPs), $\bar{P}(\tau)$, as the square magnitude of the impulse responses averaged over snapshots and antennas.[4] Preceding our results section, we note that the APDP of our measurements can be well described by a single-exponential (SE) decay, i.e., $\bar{P}(\tau) = \bar{P}_0 e^{-\tau/\gamma}$ where γ is the decay time constant. An important and convenient implication of the SE decay model, is that decay time constant equals the rms delay spread of the channel (defined as the second central moment of the APDP; see e.g., [15]). We therefore choose to extract the decay time constant instead of the rms delay spread, because it is less sensitive to noise floor influence [21]. The decay constant values are extracted by fitting regression lines to the APDPs on a dB scale.

IV. RESULTS

A. Pathloss and Shadowing

The (deterministic) distance dependent power decay is modeled, in dB, as

$$ G_{\text{det}}(d) = G_0 - 10n \log_{10}(d/d_0), \qquad (4) $$

where G_0 is the path gain at a distance $d_0 = 1$ m and n is the pathloss exponent. Fig. 3 shows a scatter plot of the total and local path gain, $G_{\text{tot}}(d)$ and $G_i(d, o)$, respectively, along with a fit of $G_{\text{tot}}(d)$ to Eq. (4) for the 5.2 GHz HH$_6$ to HH$_6$ LOS measurements. We draw two important conclusions from the figure: (i) our theory of two types of shadowing is confirmed – the local power variations of $G_i(d, o)$ around $G_{\text{tot}}(d)$ can be clearly seen from the figure; (ii) the distance dependence is weak, compared to the variations around it – for scenarios with a low pathloss exponent, the signal attenuation due to the antenna direction can prove to be a factor of greater importance than the signal attenuation due to increasing distance. The extracted pathloss exponent is between 0.2 and 1.4 for all but one LOS scenarios, whereas for NLOS scenarios, the distance dependence is stronger, with pathloss exponents between 1.7 and 2.7.

The shadowing loss L_e due to the environment is found to be reasonably well described by a log-normal distribution (i.e., by using a χ^2–test with a 1% significance level, we find that the dB values of L_e can be described as Gaussian with a standard deviation σ_{L_e}) as can be seen in Fig. 4. Another χ^2–test with the same significance level reveals that the dB values of the body shadowing loss L_b also can be described by a Gaussian distribution, with a standard deviation σ_{L_b} (see Fig. 4). The pathloss and shadowing model parameters are given in Table II, and from the table we note that the body shadowing variance is constant irrespective of whether the measurement is LOS or NLOS. Also, with the exception of the HH to HH scenario, all model parameters are fairly constant over the two frequency ranges. Furthermore, by comparing

[4]By averaging over the antenna elements, we thus choose to neglect the aforementioned influence of the antenna arrangements in this part of the analysis.
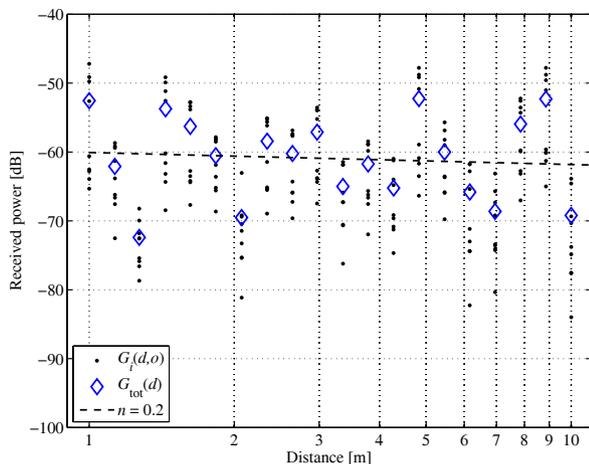
Fig. 3. Scatter plot of the received power vs. distance for the 5.2 GHz HH_6 to HH_6 LOS measurements.

Fig. 5. Correlation between body shadowing loss and decay time constant for the 5.2 GHz HH_3 to HH_4 LOS measurements. The correlation coefficient in this case is 0.56.
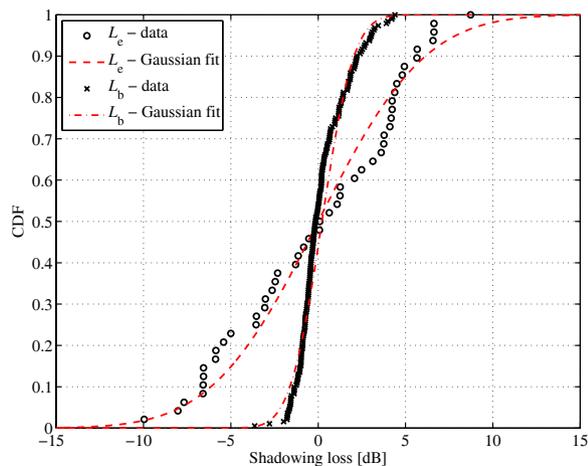

Fig. 4. Cdf:s of the shadowing loss due to the environment, L_e, and the body shadowing loss, L_b, for the 5.2 GHz AP to HH_6 NLOS measurements.

the results of e.g., $AP2HH_3^{5.2}$ and $AP2HH_6^{5.2}$, we note that the difference between the different types of handheld devices is small, even though they use different antenna types as well as array design.

B. Power Delay Profile

Since it has previously been reported in the literature [22] that delay spread and shadow fading are correlated, we seek to investigate if this is the case for both types of shadowing. Noting that the APDP of our measurements consists of a single, exponentially decaying cluster,[5] we thus evaluate this, following the reasoning from Sec. III-C, by deriving the correlation between the two types of shadowing and the decay time constant γ instead.

The results reveal that there is (with one exception) a positive correlation between both types of shadowing and the

[5]Note that due to the idiosyncrasies of measuring PAN channels, it is not possible to use the angular domain for a more refined identification of clusters.
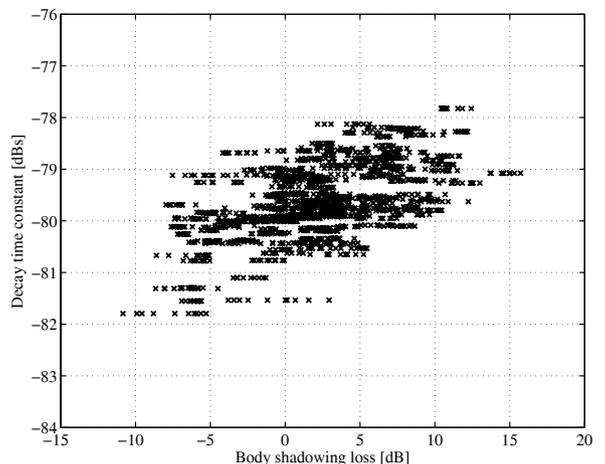
delay spread for all measured scenarios, i.e., the shadowing loss increases for increasing delay spread (see Fig. 5). Excluding the 2.6 GHz HH to HH scenario (which has a correlation coefficient of -0.12), the correlation coefficient between $L_e|_{dB}$ and $\gamma|_{dB}$ lie between $0.32 - 0.78$ for LOS and $0.16 - 0.54$ for NLOS, whereas the correlation coefficients between $L_b|_{dB}$ and $\gamma|_{dB}$ lie between $0.26 - 0.58$ for LOS and $0.17 - 0.40$ for NLOS.

Returning to the decay time constant, we do not see any distance dependence, as has been reported in previous measurement campaigns [22], but instead choose to model γ as a random variable. Using a χ^2–test with a 5% significance level, we find that within each scenario, the variations of the decay time constant *in dB* can be well described by a Gaussian distribution (see Fig. 6). We thus have $\gamma|_{dB} \sim N(m_\gamma, \sigma_\gamma)$ with constant values given by Table II. We note that there is essentially no difference between different scenarios, which is reasonable since the delay spread of the channel is mainly determined by the environment and not the antenna arrangements.

C. Small-Scale Fading Statistics

A study of the histograms of the received amplitudes (using frequency subchannels *and* snapshots) for the different spatial channels of a measurement, allows us to draw two conclusions: (i) *within the same measurement*, the statistics of different spatial channels can be quite different, and (ii) the Rice and Rayleigh distributions cannot completely describe it. Fig. 7 shows the statistics for the 3×4 spatial channels of a LOS measurement from the 5.2 GHz HH_3 to HH_4 scenario (using frequency subchannels *and* spatial snapshots as ensemble). Comparing with the best-fit Rice and Rayleigh distributions (also plotted for each ensemble), we note that, within the same *LOS* measurement, only a few spatial channels are well described by a Rice distribution (with a reasonably high K–factor), whereas others are better described by a Rayleigh. Since the antenna patterns are fairly directive (and with the placement of the antenna elements in mind), a
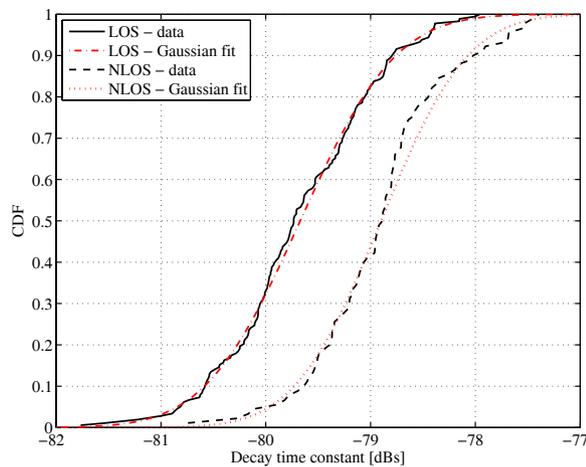
Fig. 6. Cdf:s of the decay time constants γ from the 2.6 GHz HH to HH scenario, LOS as well as NLOS data.
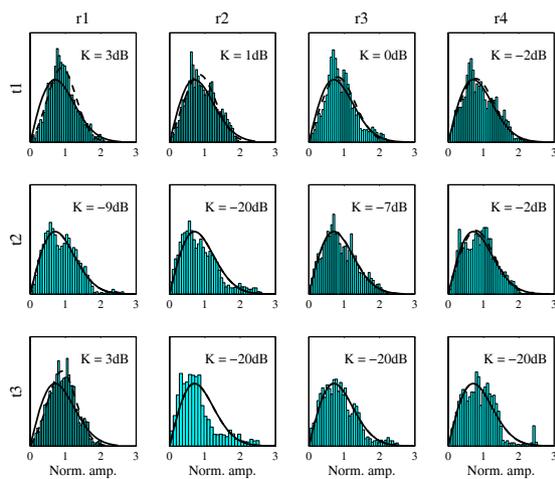

Fig. 8. Cdf:s of the snapshot amplitude statistics for one spatial channel from the 5.2 GHz, HH_3 to HH_4, Tx3 to Rx9 measurement. The solid lines are measured data, the dashed lines are best fit Ricean distributions (with the ML $K-$factor given), whereas the dotted lines are best fit Rayleigh distributions. It is clearly seen that different snapshots have different statistics.

Fig. 7. Amplitude statistics for all spatial channels from the 5.2 GHz, HH_3 to HH_4, Tx4 to Rx18 measurement (see Fig. 2). The figure is organized as a matrix with Tx elements (t1, t2,...) as rows and Rx elements as columns (r1, r2,...; the indices are written in the left and top perimeter). For each ensemble (snapshots *and* frequency samples), a Ricean fit (dashed; with the ML K-factor given) and a Rayleigh fit (solid) is shown.

possible explanation for the lack of Ricean channels can be that the antenna gain in the direction of the optical LOS is very poor for some antenna elements, and hence the signal strength of the optical LOS path becomes weak compared to the reflected paths. However, and more importantly, we also note that some channels are poorly described by a Rayleigh as well as a Ricean (e.g., t3 to r2 in Fig. 7).

To get further insight into the cases that are, clearly, neither Ricean nor Rayleigh, we investigate the amplitude statistics of each snapshot separately, i.e., we use *only* the (321) frequency subchannels as the ensemble for analysis. The results show that there is also a clear difference in the statistics of different *snapshots*, where some are well described by a Rice distribution, whereas others are better described by a Rayleigh distribution. Thus the total small-scale amplitude variations over the snapshots becomes a mixture of Rice and Rayleigh
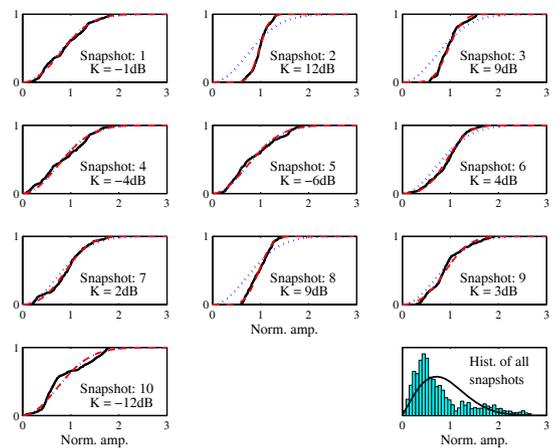
samples. The shifting between Ricean and Rayleigh would be obvious for cases where either of the antenna device holders are facing away from the other, and the small motion of the Tx device could make the optical LOS path between the antennas alternate between unobstructed during some snapshots, and obstructed by the body of the device holder during others. However, this effect is also present in measurements were both human bodies are clearly out of the way. Fig. 8 shows cdf:s of the snapshot amplitude distributions from a LOS measurement (again from the 5.2 GHz, HH_3 to HH_4 scenario) where Tx and Rx are separated by only 1 m and the device holders are facing each other. We note that snapshots 2, 3 and 8 appear Ricean distributed while the others rather are Rayleigh distributed. A possible explanation for this could be the directivity of the antenna elements and the influence of the device holder's arm. Since the arm in practice becomes a part of the antenna, the radiation pattern is likely to change slightly with the small-scale movement of the device, and hence, the antenna gain in the optical LOS will change from snapshot to snapshot.

It is thus a noteworthy result from our measurements that the statistics of the ensemble created by the different frequency samples are different from the statistics of the ensemble created by also using the snapshot (or temporal) samples. Consequently, the concept of frequency ergodicity, as introduced by Kattenbach [23], becomes invalid in this case. With only 10 spatial samples available, a complete model for the $K-$factor variations cannot be derived in a satisfactory way. However, by looking at the variations of the *mean* and *standard deviation* of the ML estimated $K-$factor (in dB) within each spatial channel, denoted $\bar{K}_{dB}$ and $\sigma_{K_{dB}}$, respectively, we can make a coarse analysis of the $K-$factor fluctuations. The mean of $\sigma_{K_{dB}}$, over spatial channels and measurement positions, is varying between 4.5 and 6.0 dB for the different LOS scenarios and between 4.9 and 5.6 dB for the NLOS scenarios, and we thus note that the $K-$factor variations within a spatial channel generally are high.

The mean value of $\bar{K}_{dB}$ is varying between -2.2 and 1.5 dB for the LOS scenarios whereas the mean value for the NLOS scenarios lie between -3.8 and -1.5 dB.

For many applications, it is still of interest to consider the statistics of the ensemble of snapshots and frequency. Thus, the amplitude data is fitted to a Rayleigh distribution, a Rice distribution and a GG distribution and we determine which distribution that best describe each ensemble by using the Akaike weights as described in Sec. III-B. Using the distribution with the highest weight (i.e., probability of being the best fit) as test outcome, we conclude that the GG distribution is regarded as the best fit in a clear majority of the cases (around $60-70\%$), whereas the remainder of the test outcomes are evenly spread over Ricean and Rayleigh. For those reasons, we use the GG distribution model the small-scale statistics and thus focus on how to select the distribution parameters.

As previously mentioned, the GG distribution is controlled by the three parameters, α, β and c, where c controls the upper part of the pdf, and αc controls the lower part. It can be shown [18] that

$$\beta = \sqrt{E\left(r^2\right)\frac{\Gamma\left(\alpha\right)}{\Gamma\left(\alpha + 2/c\right)}} = \sqrt{\frac{\Gamma\left(\alpha\right)}{\Gamma\left(\alpha + 2/c\right)}} \qquad (5)$$

where the last equality stems from the fact that we use normalized data. Since this relation is maintained in the ML estimation process, we have $\beta = \beta\left(\alpha, c\right)$ and thus only need a model for α and c.

While there might be correlation between the fading of adjacent spatial channels, this aspect is beyond the scope of the current paper where we restrict ourselves to modeling the fading of a single link. No significant correlation is found between the small-scale parameters (α, c and the relative path gain G_r) and the two shadowing types or the Tx-Rx separation, but by using a χ^2–test with a 5% significance level, we find that for each spatial subchannel, the *dB-values* of α and c can be well described as (strongly) correlated Gaussian random variables (see Figs. 9 and 10).[6] Another χ^2–test shows that G_r *in dB* also can be described by a Gaussian (see Fig. 9), and since we do not find any correlation between G_r and α or c, we choose our model as

$$\begin{bmatrix} \alpha & c & G_r \end{bmatrix}^T \sim \mathcal{N}\left(\mu, \mathbf{C}\right) \qquad (6)$$

with a mean value matrix

$$\mu = \begin{bmatrix} \mu_\alpha & \mu_c & \mu_{G_r} \end{bmatrix}^T \qquad (7)$$

and a covariance matrix

$$\mathbf{C} = \begin{bmatrix} R_{\alpha\alpha} & R_{\alpha c} & 0 \\ R_{\alpha c} & R_{cc} & 0 \\ 0 & 0 & R_{G_r G_r} \end{bmatrix}. \qquad (8)$$

Parameter values for the small-scale fading model, derived as the average over all spatial channels within each scenario, are given in Table II.

[6] In a few cases ($< 1\%$ of the outcomes), the ML estimation process failed to create meaningful results, by means of leading to a monotonically decreasing log-likelihood function (for an increasing c). Thus, the smallest value of the c-stepping range (0.1 in our case) was returned from the estimator, and as these results are obviously unphysical, they were disregarded in the analysis.
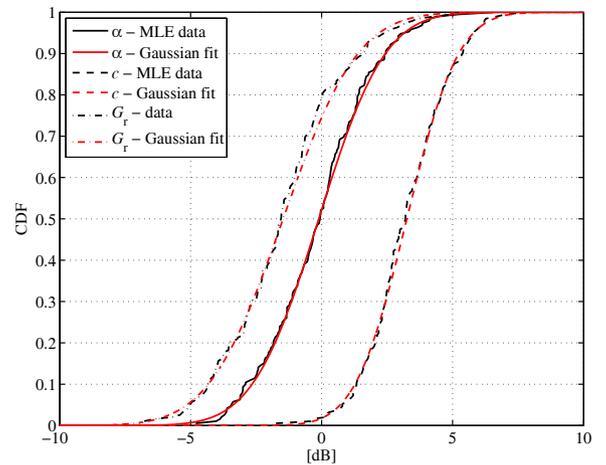

Fig. 9. Extracted smallscale parameters for one spatial channel of the 5.2 GHz AP to HH$_6$ NLOS measurements. Also shown are Gaussian fits to the data.
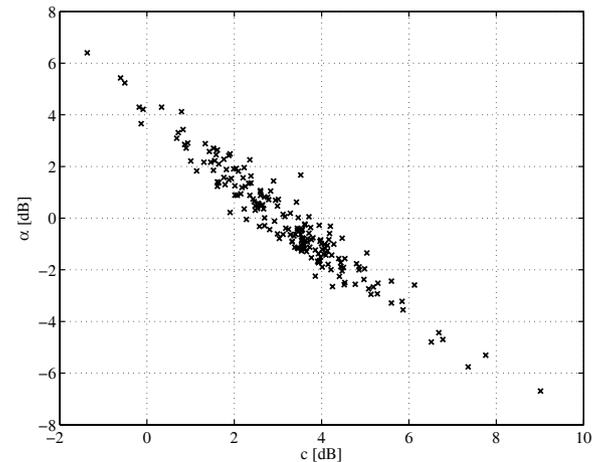

Fig. 10. ML estimates of α and c for one spatial channel of the 5.2 GHz AP to HH$_6$ NLOS measurements.

The model is thus based on the observation that the irregular antenna arrangements create unpredictable small-scale fading statistics, an observation that is true for all but one of the measured scenarios – the AP to BW scenario. This is not surprising, since this is a scenario where neither Tx nor Rx does in fact have an irregular antenna arrangement, rather all spatial channels can be characterized as co- or crosspolarized. Hence this scenario implies fading statistics that are far more predictable, and therefore this scenario is left out of our model.

V. OUR MODEL

A realization of the complete path gain (in dB) for the spatial channel between Tx element n and Rx element m separated by a distance d is thus given by

$$G\left(d, m, n\right) = G_0 - 10n\log_{10}\left(\frac{d}{d_0}\right) - L_e - L_b + G_r + G_{ss} \qquad (9)$$

where L_e, L_b, and G_r has been defined previously, and $\sqrt{G_{ss}}$ is the small-scale amplitude drawn from the generalized gamma

TABLE II
MODEL PARAMETERS.

LOS	G_0	n	σ_{L_e}	σ_{L_b}	μ_α	μ_c	μ_{G_r}	$R_{\alpha\alpha}$	$R_{\alpha c}$	R_{cc}	$R_{G_rG_r}$	m_γ	σ_γ	ρ_{L_e}	ρ_{L_b}
AP2HH$^{2.6}$	-43	1.4	2.3	2.3	-0.7	4.3	-0.6	8.4	-5.1	3.9	4.8	-80	0.4	0.6	0.4
PC2HH$^{2.6}$	-54	0.6	6.4	2.7	-0.2	3.6	-0.5	7.1	-4.0	3.3	4.0	-80	0.8	0.3	0.3
HH2HH$^{2.6}$	-47	2.7	4.2	4.2	0.1	3.1	-0.6	5.5	-3.6	2.7	3.7	-80	0.7	-0.1	0.6
AP2HH$^{5.2}_6$	-47	1.0	2.4	1.7	-0.2	4.0	-1.5	8.5	-4.5	3.4	12	-80	0.4	0.8	0.3
AP2HH$^{5.2}_4$	-47	1.2	2.7	2.2	-0.1	3.6	-1.4	6.7	-4.0	3.3	11	-80	0.4	0.7	0.3
PC2HH$^{5.2}_6$	-59	0.6	5.5	2.9	-0.1	3.6	-1.6	10	-5.8	4.5	13	-80	0.8	0.6	0.4
PC2HH$^{5.2}_4$	-60	0.7	5.4	3.7	0.2	3.2	-1.2	10	-6.2	4.5	9.2	-80	0.8	0.4	0.4
HH2HH$^{5.2}_6$	-60	0.2	6.2	5.5	0.3	3.1	-2.3	7.5	-4.2	3.2	21	-80	0.8	0.5	0.6
HH2HH$^{5.2}_4$	-60	0.3	6.3	4.6	0.4	2.9	-1.1	7.1	-4.6	3.4	8.7	-80	0.7	0.6	0.6
NLOS															
AP2HH$^{2.6}$	-48	2.0	5.1	2.2	-0.4	3.5	-0.6	6.0	-4.1	3.1	4.0	-79	0.6	0.5	0.2
HH2HH$^{2.6}$	-55	2.2	3.6	3.6	0.3	2.9	-0.4	4.3	-2.9	2.2	2.7	-79	0.6	0.4	0.4
AP2HH$^{5.2}_6$	-54	1.7	4.8	1.5	0.0	3.2	-1.2	4.9	-3.2	2.4	8.9	-79	0.5	0.5	0.2
AP2HH$^{5.2}_4$	-54	1.8	4.7	2.1	0.3	2.9	-0.7	5.1	-3.3	2.4	5.8	-79	0.5	0.4	0.2
HH2HH$^{5.2}_6$	-53	2.6	2.9	4.3	0.6	2.7	-1.7	4.8	-3.1	2.3	15	-79	0.7	0.2	0.4
HH2HH$^{5.2}_4$	-53	2.7	2.7	3.6	1.1	2.2	-2.3	6.0	-4.1	2.9	14	-79	0.7	0.2	0.3

distribution. How to generate data can be summarized as follows:

1) For each Tx-Rx separation d, derive the deterministic path gain from Eq. (4), and subtract a shadowing loss caused by the environment, $L_e \sim \mathcal{N}(0, \sigma_{L_e})$.

2) Next, for every simulated orientation of a user, subtract an additional body shadowing loss $L_b \sim \mathcal{N}(0, \sigma_{L_b})$.

3) For each (uncorrelated) spatial channel, add a relative gain G_r and derive the pdf of its small-scale statistics by drawing α, c and G_r according to Eq. (6). Finally, to account for the small-scale effects, add a small-scale channel gain G_{ss} by generating $\sqrt{G_{ss}}$ from the generalized gamma pdf determined by α, c and β, where the latter is given by Eq. (5).

Additionally, the model can be extended by deriving a SE power delay profile with a Gaussian distributed decay constant (in dBseconds) having a correlation to both types of shadowing.

A. Validation of Model

To verify the agreement of model and measurements, we derive, for each scenario, the same number of channel realizations as measured, and compare with the measured results. The metrics we use for comparison are cdf:s of the simulated received power, evaluated for four cases: (i) averaged over frequency, (ii) averaged over frequency and spatial channels, (iii) averaged over frequency, spatial channels and rotations, and (iv) without averaging. We find that the agreement between measurements and model is very good, as can be seen in Fig. 11, where simulation results for the 5.2 GHz HH$_3$ to HH$_4$ scenario are displayed.

VI. SUMMARY AND CONCLUSIONS

We have reported results from an extensive channel measurement campaign, where scenarios, antenna arrangements, and choice of locations have been selected in order to correspond to typical PANs. Measurements were performed over two frequency ranges, using a multitude of multi-antenna devices combined in various ways to create several different
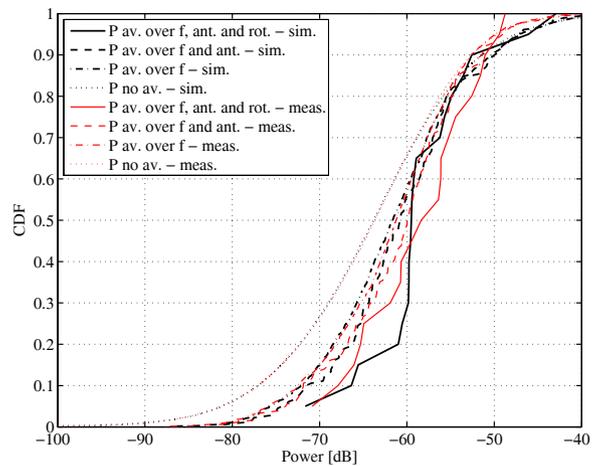

Fig. 11. Comparison of modeled and measured power for the 5.2 GHz HH$_3$ to HH$_4$ LOS scenario.

scenarios. Our results show that PAN channels exhibit fundamental differences in the structure of large-scale as well as small-scale fading statistics, namely that:

- Due to the impact of the irregular antenna arrangements and the impact of the (antenna device) users typically involved in PANs, the small-scale varying amplitude is sensitive to even very small movements. Hence, a spatial channel is likely to fluctuate between "seeing" a Rayleigh and a Ricean environment, and thus the small-scale amplitude variations over a small area cannot be described by the Rayleigh our Rice distribution alone. Rather a mixed distribution has to be used; in this paper we have used the generalized gamma distribution as a model.

- It is suitable to distinguish between two types of shadowing; (i) body shadowing (due to the rotation of the device holder) and (ii) shadowing due to the physical environment (lateral movement).

The second observation was present in all of the measured scenarios, whereas the first was present in all scenarios except the AP to BW scenario, in which the antenna devices we

used caused far more predictable small-scale statistics. The small differences between LOS and NLOS are likely due to the little attenuation provided by the gypsum walls separating the offices of our measurement environment. Furthermore, we have noted that:

- In the distance range considered for PANs, the impact of the distance on the received power can be minor, and shadowing effects dominate, especially for LOS situations.
- The power delay profile is well described by a single exponential, with a decay time constant (i.e., delay spread) in dB described by a Gaussian distributed random variable.
- The definition of LOS becomes ambiguous, as the obstruction of a direct propagation path between Tx and Rx can be due to the direction of the antenna, or the person holding the device.
- The channel parameters do not change significantly between the 2.6 and 5.2 GHz frequency range.

We have also created and parameterized a channel model based on our observations. In the model, the two types of shadowing are given as random processes, well described by log-normal distributions. Also, both types of shadowing are found to be correlated with the delay spread. The model can be used for system design and performance prediction of PAN systems.

VII. ACKNOWLEDGEMENTS

REFERENCES

[1] J. Karedal, A. J. Johansson, F. Tufvesson, and A. F. Molisch, "Characterization of MIMO channels for handheld devices in personal area networks at 5 GHz," in *Proc. European Signal Processing Conf. 2006*, Sept. 2006.
[2] ——, "Shadowing effects in MIMO channels for personal area networks," in *Proc. IEEE Veh. Technol. Conf. 2006 Fall*, 2006.
[3] D. Bakker, D. M. Gilster, and R. Gilster, *Bluetooth End to End*, 1st ed. Wiley, 2002.
[4] A. Batra *et al.*, "Multi-band OFDM physical layer proposal," 2003, document IEEE 802.15-03/267r2.
[5] J. H. Winters, "On the capacity of radio communications systems with diversity in Rayleigh fading environments," *IEEE J. Select. Areas Commun.*, vol. 5, no. 5, pp. 871-878, June 1987.
[6] G. J. Foschini and M. J. Gans, "On limits of wireless communications in a fading environment when using multiple antennas," *Wireless Personal Commun.*, vol. 6, pp. 311-335, Feb. 1998.
[7] A. Paulraj, D. Gore, and R. Nabar, *Multiple Antenna Systems*. Cambridge, U.K.: Cambridge University Press, 2003.
[8] [Online] Available: http://www.ist-magnet.org/
[9] V. Erceg, L. Schumacher, P. Kyritsi, A. Molisch, D. S. Baum, A. Y. Gorokhov, C. Oestges, Q. Li, K. Yu, N. Tal, B. D. Dijkstra, A. Jagannatham, C. Lanzl, V. J. Rhodes, J. Medbo, D. Michelson, and M. Webster, "TGn Channel Models," IEEE P802.11 Wireless LANs, Tech. Rep., May 2004. [Online] Available: http://www.802wirelessworld.com:8802/.
[10] J. Medbo, J.-E. Berg, and F. Harryson, "Temporal radio channel variations with stationary terminal," in *Proc. IEEE Veh. Technol. Conf. 2004 Fall*, Sept. 2004, pp. 91-95.
[11] A. Alomainy, Y. Hao, and X. Hu, "UWB on-body radio propagation and system modelling for wireless body-centric networks," *IEEE Proceedings - Commun.*, vol. 153, no. 1, pp. 107-115, 2006.
[12] A. Fort, C. Desset, J. Ryckaert, P. De Doncker, L. Van Biesen, and P. Wambacq, "Characterization of the ultra wideband body area propagation channel," in *Proc. IEEE International Conf. on Ultra-Wideband*, pp. 22-27, 2005.
[13] T. Zasowski, G. Meyer, F. Althaus, and A. Wittneben, "Propagation effects in uwb body area networks," in *Proc. IEEE International Conf. Ultra-Wideband*, pp. 16-21, 2005.
[14] R. Thomae, D. Hampicke, A. Richter, G. Sommerkorn, A. Schneider, U. Trautwein, and W. Wirnitzer, "Identification of the time-variant directional mobile radio channels," *IEEE Trans. Instrumentation and Measurement*, vol. 49, pp. 357-364, 2000.
[15] A. F. Molisch, *Wireless Communications*. Chichester, West Sussex, UK: IEEE Press-Wiley, 2005.
[16] A. F. Molisch *et al.*, "IEEE 802.15.4a channel model—final report, Tech. Rep. Document IEEE 802.15-04-0662-02-004a, 2005.
[17] T. S. Rappaport, *Wireless Communications—Principles and Practices*, 2nd ed. Upper Saddle River, NJ: Prentice Hall, 2002.
[18] R. Vaughan and J. B. Andersen, *Channels, Propagation and Antennas for Mobile Communications*. London, UK: IEE, 2003.
[19] H. W. Hager and L. J. Bain, "Inferential procedures for the generalized gamma distribution," *J. American Statistical Assoc.*, vol. 65, no. 332, pp. 1601-1601, Dec. 1970.
[20] H. Akaike, "Information theory and an extension of the maximum likelihood principle," in *Breakthroughs in Statistics*, S. Kotz and N. L. Johnson, Eds. New York: Springer, 1992, vol. 1, pp. 610-624.
[21] J.-P. Rossi, "Influence of measurement conditions on the evaluation of some radio channel parameters," *IEEE Trans. Veh. Technol.*, vol. 48, no. 4, pp. 1304-1316, July 1999.
[22] L. J. Greenstein, V. Erceg, Y. S. Yeh, and M. V. Clark, "A new path-gain/delay-spread propagation model for digital cellular channels," *IEEE Trans. Veh. Technol.*, vol. 46, no. 2, pp. 477-485, May 1997.
[23] R. Kattenbach, "Characterization of time-variant indoor radio channels by means of their system and correlation functions," Ph.D. dissertation, University of Kassel, 1997.

Johan Karedal received the M.S. degree in engineering physics in 2002 from Lund University in Sweden. In 2003, he started working towards the Ph.D. degree at the Department of Electrical and Information Technology, Lund University, where his research interests are on channel measurements and modeling for MIMO and UWB systems. Johan has participated in the European research initiative "MAGNET".

Anders J Johansson received his Masters, Lic. Eng. and Ph.D. degrees in electrical engineering from Lund University, Lund, Sweden, in 1993, 2000 and 2004, respectively. From 1994 to 1997 he was with Ericsson Mobile Communications AB developing transceivers and antennas for mobile phones. Since 2005 he is an Associate Professor at the Department of Electrical and Information Technology at Lund University. His research interests include antennas, wave propagation and telemetric devices for medical implants as well as antenna systems and propagation modeling for MIMO systems. He is funding chair of the Swedish chapter of IEEE Engineering in Medicine and Technology section.

Fredrik Tufvesson was born in Lund, Sweden in 1970. He received the M.S. degree in Electrical Engineering in 1994, the Licentiate Degree in 1998 and his Ph.D. in 2000, all from Lund University in Sweden. After almost two years at a startup company, Fiberless Society, Fredrik is now associate professor at the Department of Electrical and Information Technology. His main research interests are channel measurements and modeling for wireless communication, including channels for both MIMO and UWB systems. Beside this, he also works with channel estimation and synchronization problems, OFDM system design and UWB transceiver design.

Andreas F. Molisch Andreas F. Molisch (S'89, M'95, SM'00, F'05) received the Dipl. Ing., Dr. techn., and habilitation degrees from the Technical University Vienna (Austria) in 1990, 1994, and 1999, respectively. From 1991 to 2000, he was with the TU Vienna, becoming an associate professor there in 1999. From 2000-2002, he was with the Wireless Systems Research Department at AT&T (Bell) Laboratories Research in Middletown, NJ. Since then, he has been with Mitsubishi Electric Research Labs, Cambridge, MA, USA, where he is now a Distinguished Member of Technical Staff and Chief Wireless Standards Architect. He is also professor and chairholder for radio systems at Lund University, Sweden.

Dr. Molisch has done research in the areas of SAW filters, radiative transfer in atomic vapors, atomic line filters, smart antennas, and wideband systems. His current research interests are measurement and modeling of mobile radio channels, UWB, cooperative communications, and MIMO systems. Dr. Molisch has authored, co-authored or edited four books (among them the textbook "Wireless Communications, Wiley-IEEE Press), eleven book chapters, more than 110 journal papers, and numerous conference contributions, as well as more than 70 patents.

Dr. Molisch is an editor of the IEEE TRANSACTIONS ON WIRELESS COMMUNICATIONS and co-editor of special issues of several journals. He has been member of numerous TPCs, vice chair of the TPC of VTC 2005 spring, general chair of ICUWB 2006, TPC co-chair of the wireless symposium of Globecomm 2007, TPC chair of Chinacom2007, and general chair of Chinacom 2008. He has participated in the European research initiatives "COST 231," "COST 259," and "COST273," where he was chairman of the MIMO channel working group, he was chairman of the IEEE 802.15.4a channel model standardization group, and was also chairman of Commission C (signals and systems) of URSI (International Union of Radio Scientists). Dr. Molisch is a Fellow of the IEEE, a Fellow of the IET, an IEEE Distinguished Lecturer, and recipient of several awards.